Analyses of Orthogonal and Non-Orthogonal Steering Vectors at Millimeter Wave Systems

Hsiao-Lan Chiang, Tobias Kadur, and Gerhard Fettweis
Vodafone Chair for Mobile Communications
Technische Universität Dresden
Helmholtzstrasse 18, Dresden, Germany
Email: {hsiao-lan.chiang, tobias.kadur, gerhard.fettweis}@ifn.et.tu-dresden.de

***Abstract*—Beamforming is one of the most challenging problems for millimeter wave communication. With limited codebook size, how to design the steering angles to compensate angles of arrival and departure (AoAs/AoDs) is essential to beamforming performance. Typically, two categories of steering vector sets are commonly used. One is orthogonal steering vector set where the spatial frequency indices of the steering angles are uniformly distributed in spatial frequency domain. The other one is non-orthogonal steering vector set where the steering angles are uniformly distributed in angle domain. In this paper, analyses of these two designs are presented. Due to the fact that beamwidth are constant with respect to different spatial frequency indices in spatial frequency domain, if the spatial frequency indices are uniformly distributed, one has the smallest deviation of the beamforming gain. Since the orthogonal steering vectors satisfy this condition that spatial frequency indices are uniformly distributed, they can achieve higher data rates than the non-orthogonal ones when the AoAs are uniformly distributed over $(-\frac{\pi}{2}, \frac{\pi}{2})$.**

***Index Terms*—millimeter wave, spatial frequency, analog beamforming, orthogonal steering vectors**

I. Introduction

With the rapid increase of data rate in wireless communication, bandwidth shortage is getting more critical. Therefore, there is a growing interest in using millimeter wave (mmW) for future wireless communications taking advantage of the enormous amount of available spectrum [1]. Measurements of most large and small scale parameters for mmW channels in urban areas at 73 GHz had been presented in [2]. It seems that path loss in such environment is very severe, and in order to improve capacity and service quality, mmW together with massive multiple input multiple output is a promising approach [3].

Most of today's beamforming systems operating in lower carrier frequency bands ($\leq$ 6 GHz) are based on digital beamforming (DBF) architecture. In this architecture, each antenna has its own RF chain, including digital-to-analog converter (DAC) at the transmitter and analog-to-digital converter (ADC) at the receiver. However, in order to exploit huge available bandwidth in mmW bands, ADCs and DACs have to run at served Giga samples per second. It is nearly infeasible to equip each antenna with one RF chain due to high implementation cost and power consumption. Therefore, analog beamforming (ABF) [4], [5] is adopted at mmW, which consists of multiple phase shifters connecting to one RF chain. Compared to DBF, it provides low cost solutions to implementation requirements.

978-1-5090-2185-7/16/$31.00

Due to hardware implementation cost and feedback overhead, the limited number of steering angles are predefined in the codebook. Larger size of the codebook means that more bits are needed to feedback the selected codeword [6] and more complicated requirements on phase shifters. Therefore, with limited codebook size, how to design the steering angles is important. If angles of arrival (AoAs) are uniformly distributed in angle domain, intuitively, the design of steering angles are supposed to be discrete uniformly distributed in angle domain as well. However, the work in [7] shows different results that nonuniformly distributed steering angles achieve better data rate. The argument is that in spatial frequency domain the steering spatial frequencies and the spatial frequencies of AoAs have nearly the same distribution. Nevertheless, this assumption is only valid within some range of angles. In this paper, more convincing explanations for the design of the steering vectors from different perspectives are presented.

The work in [8] presented that beamwidth does not vary with spatial frequency. According to this property, we find that when the designed steering spatial frequencies are uniformly distributed in spatial frequency domain, the maximum deviation of the beamforming gain is limited to -3 dB. On the other hand, for the nonuniformly distributed steering spatial frequencies, the maximum deviation of the beamforming gain could be greater or less than -3 dB. In the simulated data rates, it shows that when the AoAs are uniformly distributed over $(-\frac{\pi}{2}, \frac{\pi}{2})$, the averaged beamforming gain by non-orthogonal steering vectors is worse than the orthogonal ones because within some range of AoAs the beamforming gain is -10 dB worse than -3 dB gain.

This paper is organized as follows: In Section II, we describe the system models. Section III elaborates the signals in angle and spatial frequency domain. Also, orthogonal and non-orthogonal steering vectors are discussed in spatial frequency domain. Simulation results are presented in Section IV, and we conclude our work in Section V.

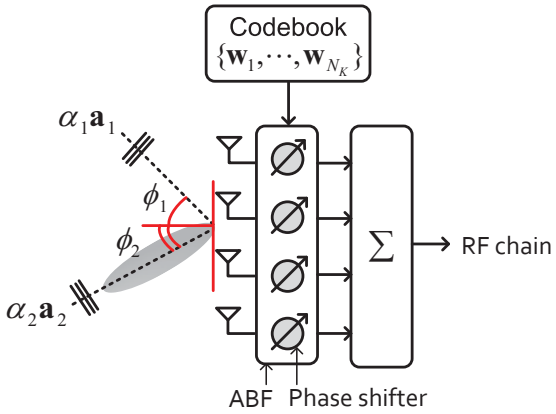

Figure 1: A diagram of one ABF system with four antenna elements at the receiver in a sparse mmW channel with two AoAs.

II. System Models

Fig. 1 shows a diagram of the ABF system with N_R antennas at the receiver. An $N_R \times 1$ steering vector $\mathbf{w}_k$ is selected from the codebook, which consists of N_K steering vectors $\{\mathbf{w}_1, \cdots, \mathbf{w}_{N_K}\}$. Each steering vector can be expressed as

$$\mathbf{w}_k = \frac{1}{\sqrt{N_R}} \left[1, e^{j2\pi\lambda_0^{-1}\sin\phi_k\Delta_d}, \cdots, e^{j2\pi\lambda_0^{-1}\sin\phi_k(N_R-1)\Delta_d}\right]^T, \tag{1}$$

where $k = 1, \cdots, N_K$, ϕ_k is the k^{th} steering angle, $\Delta_d \triangleq \frac{\lambda_0}{2}$ is the distance between two antenna elements, and λ_0 is the wavelength at the carrier frequency. In (1), the term $\lambda_0^{-1}\sin\phi_k$ is referred to as a steering spatial frequency with respect to the steering angles ϕ_k. $(\cdot)^T$ denotes transpose of a matrix.

Different to Rayleigh/Rician fading channel models, which are often assumed for centimeter wave (cmW) communication, mmW channel models show sparsity of AoAs and AoDs between transmitter and receiver due to severe path loss [2]. Therefore, beam steering plays an important role at mmW systems. To deal with both AoDs and AoAs at the same time is a huge challenge because all the combinations of the beamformers at the transmitter and the receiver have to be considered. Accordingly, one can adopt an omni-directional antenna at the transmitter, as introduced in IEEE 802.11ad [9], to simplify the beamforming procedure. Then the receiver, equipped with a uniform linear array (ULA) antenna, only experiences multiple AoAs as shown in Fig. 1, where two AoAs are assumed in the mmW environment.

The received signal before RF chain can be formulated as

$$r_k = s \cdot \sum_{p=0}^{N_P-1} \alpha_p \mathbf{w}_k^H \mathbf{a}_p + \mathbf{w}_k^H \mathbf{z}, \tag{2}$$

where $\mathbf{w}_k^H$ denotes Hermitian transpose of $\mathbf{w}_k$, r_k is the received signal with respect to the k^{th} steering vector, s is the transmitted signal satisfying $\mathbb{E}[|s|^2] = 1$, $\alpha_p \in \mathbb{C}^{1\times 1}$ is the complex attenuation coefficient for path p, and $\mathbf{z}$ is an $N_R \times 1$ additive white Gaussian noise (AWGN) vector with the element $z_{n_r} \sim \mathcal{CN}(0, \sigma_z^2)$, $n_r = 0 \cdots, N_R - 1$. N_P is the number of channel paths. $\mathbf{a}_p$ is an $N_R \times 1$ array propagation vector [5] with respect to the p^{th} AoA ϕ_p, which can be represented as

$$\mathbf{a}_p = \frac{1}{\sqrt{N_R}} \left[1, e^{j2\pi\lambda_0^{-1}\sin\phi_p\Delta_d}, \cdots, e^{j2\pi\lambda_0^{-1}\sin\phi_p(N_R-1)\Delta_d}\right]^T, \tag{3}$$

where $\lambda_0^{-1}\sin\phi_p$ is the channel spatial frequency with respect to the AoA ϕ_p.

III. The Analyses of Orthogonal and Non-orthogonal Steering Vectors

A. Spatial Frequency Index

By introducing a spatial frequency scaling factor defined as $\Delta_\nu \triangleq 1/(N_R\Delta_d)$ [10], the spatial frequency index (or normalized spatial frequency) with respect to the steering angle ϕ_k is defined as

$$\underbrace{\nu_k}_{\text{spatial frequency index}} \triangleq \underbrace{\frac{\sin\phi_k}{\lambda_0}}_{\text{spatial frequency}} \cdot \frac{1}{\Delta_\nu} = \frac{N_R \cdot \sin\phi_k}{2}. \tag{4}$$

Given a spatial frequency index ν_k, the steering vector in (1) can be rewritten as

$$\mathbf{w}_k = \frac{1}{\sqrt{N_R}} \left[1, e^{j2\pi\nu_k/N_R}, \cdots, e^{j2\pi\nu_k(N_R-1)/N_R}\right]^T. \tag{5}$$

B. Orthogonal and Non-Orthogonal Steering Vectors

The steering vectors with uniformly distributed spatial frequency indices are called orthogonal steering vectors, such as Butler matrix [11]. To be formal, one defines the orthogonality of any two steering vectors as

$$\frac{\langle \mathbf{w}_i, \mathbf{w}_j \rangle}{||\mathbf{w}_i||_2 \cdot ||\mathbf{w}_i||_2} = \begin{cases} 0, & i \neq j \\ 1, & i = j \end{cases}, \tag{6}$$

where $\langle \mathbf{w}_i, \mathbf{w}_j \rangle$ denotes inner product of two vectors. Given the number N_R of antennas, the N_K (assume that $N_K = N_R$) spatial frequency indices are shown as [11]

$$\nu_k = \begin{cases} \pm 0.5, \pm 1.5, \cdots, \pm\frac{N_R-1}{2}, & \text{if } N_K \text{ is an even number} \\ 0, \pm 1, \pm 2, \cdots, \pm\frac{N_R-1}{2}, & \text{if } N_K \text{ is an odd number} \end{cases}. \tag{7}$$

The other way to design the steering vectors is having the uniformly distributed steering angles over the range of the scanning angles. From the relationship between the steering angles and the corresponding spatial frequency indices in (4), we know that the steering spatial frequency indices $\{\nu_k | k = 1, \cdots, N_K\}$ are not uniformly distributed, which are different to (7). This kind of steering vectors belong to non-orthogonal steering vector set.

C. Beam Patterns Shown in Angle and Spatial Frequency Domain

Given the steering angle ϕ_k and the AoA ϕ_p, the beam pattern is defined as [5]

$$\begin{aligned}\beta_{p,k} &= \mathbf{w}_k^H \mathbf{a}_p \\ &= \frac{1}{N_R} \cdot \sum_{n_r=0}^{N_R-1} e^{j2\pi\lambda_0^{-1}(\sin\phi_p - \sin\phi_k)n_r\Delta_d} \\ &= \frac{e^{j\pi\lambda_0^{-1}\Delta_d(N_R-1)(\sin\phi_p - \sin\phi_k)}}{N_R} \times \\ &\quad \frac{\sin(\pi\lambda_0^{-1}\Delta_d N_R(\sin\phi_p - \sin\phi_k))}{\sin(\pi\lambda_0^{-1}\Delta_d(\sin\phi_p - \sin\phi_k))}. \end{aligned} \tag{8}$$

Based on the received signals $\{r_k | k = 1, \cdots, N_K\}$, the goal of beamforming is to achieve the maximal SNR [7][12]. Due to the assumption that the noise is signal-independent, the codeword (or steering vector index) can be selected according to the following equations

$$\begin{aligned}\hat{k} &= \arg \max_{k=1,\ldots,N_K} |r_k|^2 \\ &= \arg \max_{k=1,\ldots,N_K} \left| s \cdot \sum_{p=0}^{N_P-1} \alpha_p \mathbf{w}_k^H \mathbf{a}_p \right|^2 \\ &= \arg \max_{k=1,\ldots,N_K} \left| s \cdot \sum_{p=0}^{N_P-1} \alpha_p \beta_{p,k} \right|^2. \end{aligned} \tag{9}$$

To clearly explain the difference between the orthogonal and the non-orthogonal steering vectors, $N_P = 1$ is assumed in (9) in order to analyzing the beam patterns by the orthogonal and the non-orthogonal steering vectors. Therefore, (9) becomes

$$\begin{aligned}\hat{k} &= \arg \max_{k=1,\ldots,N_K} |s \cdot \alpha_p \beta_{p,k}|^2 \\ &= \arg \max_{k=1,\ldots,N_K} |\beta_{p,k}|^2, \; p = 0, \end{aligned} \tag{10}$$

where

$$|\beta_{p,k}|^2 = \frac{1}{N_R^2} \cdot \frac{\sin^2(\pi\lambda_0^{-1}\Delta_d N_R(\sin\phi_p - \sin\phi_k))}{\sin^2(\pi\lambda_0^{-1}\Delta_d(\sin\phi_p - \sin\phi_k))}. \tag{11}$$

(11) can also be represented as a function of the spatial frequency index,

$$|\beta_{p,k}|^2 = \frac{1}{N_R^2} \cdot \frac{\sin^2(2\pi\lambda_0^{-1}\Delta_d(\nu_p - \nu_k))}{\sin^2(\frac{2\pi\lambda_0^{-1}\Delta_d}{N_R}(\nu_p - \nu_k))}. \tag{12}$$

Fig. 2(a) and 2(b) illustrate beam patterns in angle and spatial frequency domain respectively with $N_R = 16$, range of AoAs is $-90^o < \phi_p < 90^o$ ($-8 < \nu_p < 8$), and the steering angles equal to $\phi_k = 0^o$, 60^o ($\nu_k = 0, 6.93$). It is obvious that in Fig. 2(a) the beamwidth varies with steering angle. The beamwidth at $\phi_k = 60^o$ is wider than the beamwidth at $\phi_k = 0^o$. Considering a angle shift $\Delta\phi$ in (11), $-90^o < \Delta\phi < 90^o$, the beam pattern (11) becomes

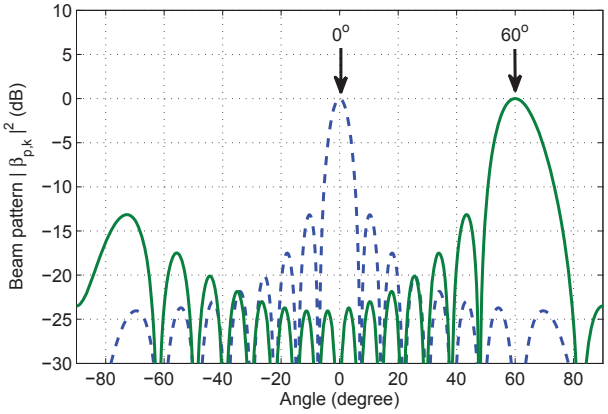

(a) Two beam patterns shown as the function of angle have different beamwidth.

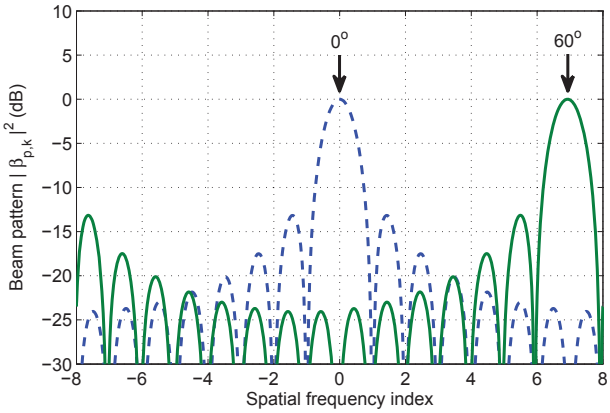

(b) Two beam patterns shown as the function of spatial frequency index have the same beamwidth.

Figure 2: Typical examples of two beam patterns represented in angle and spatial frequency domain respectively.

$$|\beta'_{p,k}|^2 = \frac{1}{N_R^2} \cdot \frac{\sin^2(\pi\lambda_0^{-1}\Delta_d N_R(\sin(\phi_p + \Delta\phi) - \sin(\phi_k + \Delta\phi)))}{\sin^2(\pi\lambda_0^{-1}\Delta_d(\sin(\phi_p + \Delta\phi) - \sin(\phi_k + \Delta\phi)))}, \tag{13}$$

which is not equal to $|\beta_{p,k}|^2$ in (11) when $\Delta\phi \neq 0$.

On the other hand, in Fig. 2(b), the beamwidth does not vary with spatial frequency index [8]. Similarly, consider a spatial frequency index shift $\Delta\nu$ in (12), $-8 < \Delta\nu < 8$, the beam pattern (12) becomes

$$\begin{aligned}|\beta'_{p,k}|^2 &= \frac{1}{N_R^2} \cdot \frac{\sin^2(2\pi\lambda_0^{-1}\Delta_d((\nu_p + \Delta\nu) - (\nu_k + \Delta\nu)))}{\sin^2(\frac{2\pi\lambda_0^{-1}\Delta_d}{N_R}((\nu_p + \Delta\nu) - (\nu_k + \Delta\nu)))} \\ &= \frac{1}{N_R^2} \cdot \frac{\sin^2(2\pi\lambda_0^{-1}\Delta_d(\nu_p - \nu_k))}{\sin^2(\frac{2\pi\lambda_0^{-1}\Delta_d}{N_R}(\nu_p - \nu_k))}, \forall\Delta\nu. \end{aligned} \tag{14}$$

Thus $|\beta'_{p,k}|^2$ in (14) is always equal to $|\beta_{p,k}|^2$ in (12) with different value of $\Delta\nu$. It can be concluded that no matter what

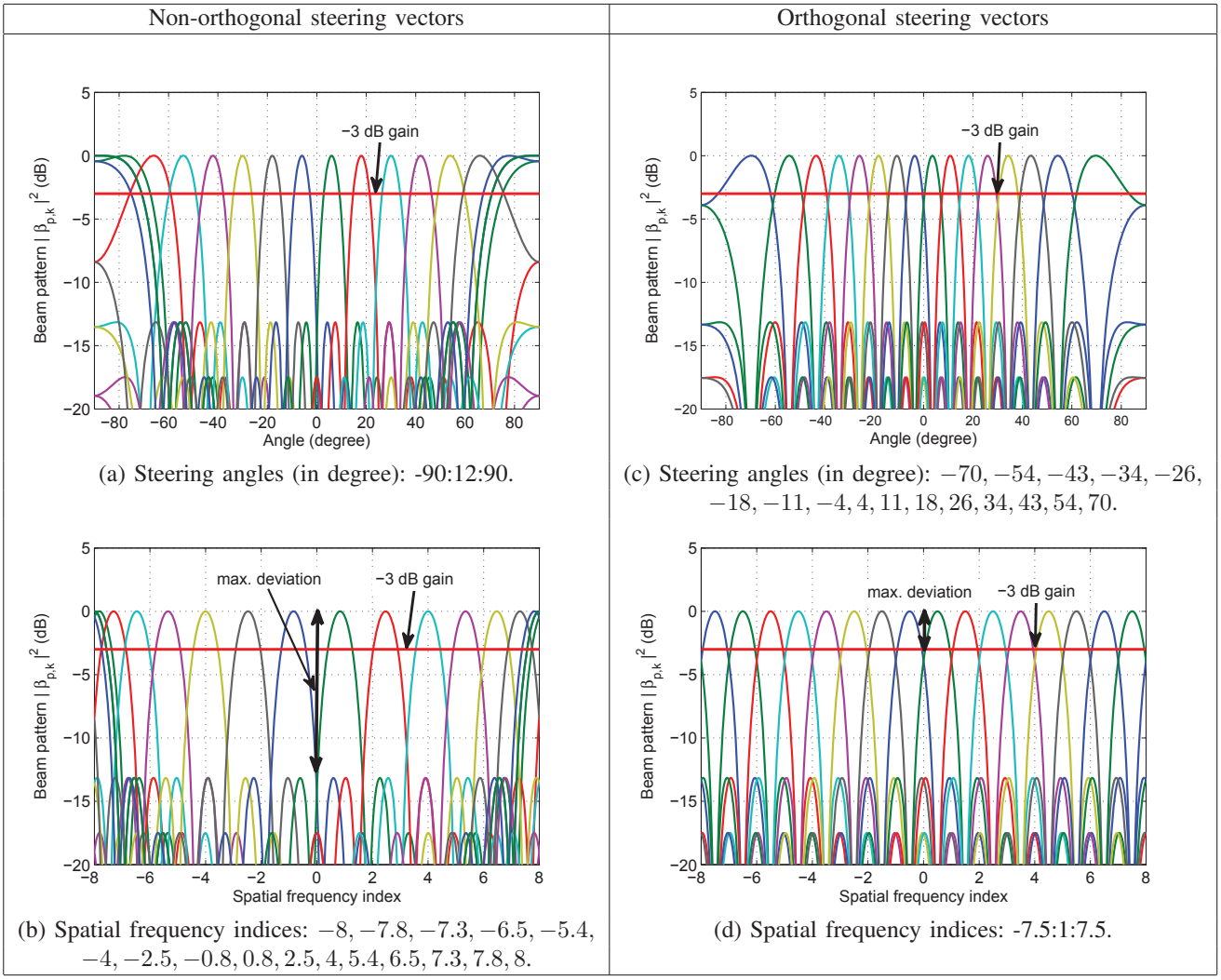

(a) Steering angles (in degree): -90:12:90.

(c) Steering angles (in degree): $-70, -54, -43, -34, -26, -18, -11, -4, 4, 11, 18, 26, 34, 43, 54, 70$.

(b) Spatial frequency indices: $-8, -7.8, -7.3, -6.5, -5.4, -4, -2.5, -0.8, 0.8, 2.5, 4, 5.4, 6.5, 7.3, 7.8, 8$.

(d) Spatial frequency indices: -7.5:1:7.5.

Figure 3: Beam patterns of the non-orthogonal and the orthogonal steering vectors shown in angle and spatial frequency domain with $N_R = 16$ and $N_K = 16$.

value of $\Delta\nu$ is, the beam pattern shifted to $\nu_k + \Delta\nu$ always keeps the same beamwidth.

When $\phi_p \sim \mathcal{U}(-\frac{\pi}{2}, \frac{\pi}{2})$, the probability density function (pdf) of ν_p ($\nu_p = \frac{N_R \cdot \sin\phi_p}{2}$) is given by (see the Appendix)

$$f_{\nu_p}(\nu_p) = \begin{cases} 0, & \nu_p < -\frac{N_R}{2} \\ \frac{2}{\pi N_R \sqrt{1-(\frac{2\nu_p}{N_R})^2}}, & -\frac{N_R}{2} \le \nu_p < \frac{N_R}{2} \\ 0, & \nu_p \ge \frac{N_R}{2} \end{cases}, \quad (15)$$

which is not uniformly distributed. In [7], the argument that the orthogonal steering vectors show higher data rates is because the spatial frequencies of the given AoAs and the orthogonal steering angles have nearly the same distribution, i.e., uniform distribution. However, this argument only holds under some assumptions.

Different opinion that the orthogonal steering vectors show higher data rate is explained as follows. In Fig. 3(b) and 3(d) the beam patterns of the non-orthogonal and the orthogonal steering vectors are shown in spatial frequency domain. The total 32 beam patterns (16 in Fig. 3(b) and 16 in Fig. 3(d)) mapping to different spatial frequency indices have the same beamwidth values, as proven in (14). Due to the property of constant beamwidth in spatial frequency domain, we analyze the difference between the orthogonal and the non-orthogonal steering vectors in spatial frequency domain.

In Fig. 3(d), the uniformly distributed spatial frequency indices lead to the results that the beamforming gain of the orthogonal steering vectors in general is larger than or almost equal to -3 dB gain. On the contrary, regarding the non-orthogonal cases in Fig. 3(b), the nonuniformly distributed spatial frequency indices result in extremely low beamforming gain at some spatial frequency indices, such as $\nu_p = 0, \pm 1.65$. Although ν_p shows lower probability within $-2 < \nu_p < 2$, the overall data rates may degrade a lot due to low beamforming gain within this interval. More simulation results are shown in Section IV. The orthogonal and the non-orthogonal beam

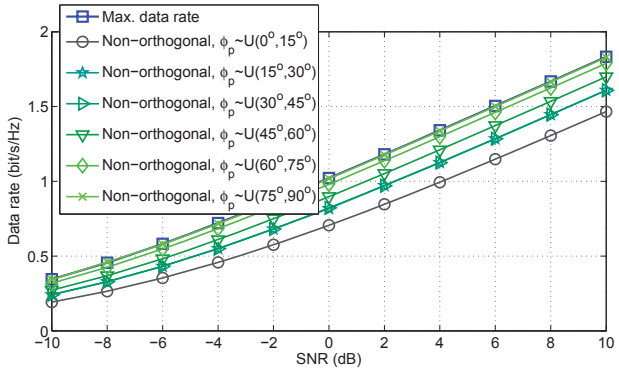

Figure 4: Comparison of achievable data rates by the perfect and the non-orthogonal steering vectors with different range of AoAs.

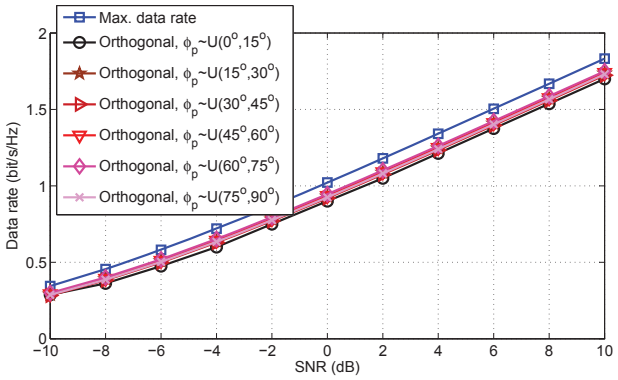

Figure 5: Comparison of achievable data rates by the perfect and the orthogonal steering vectors with different range of AoAs.

patterns shown in angle domain are illustrated in Fig. 3(a) and 3(c) for reference.

IV. Simulation Results

In the simulations, $N_R = 16$, $N_K = 16$, and $N_P = 1$ are considered. The distribution of AoA are uniformly distributed over $(-\frac{\pi}{2}, \frac{\pi}{2})$ and the channel gain is normalized to 1, $\alpha_0^2 = 1$. The simulated codebooks (consisting of N_K spatial frequency indices) for the orthogonal and the non-orthogonal steering vectors are introduced in Fig. 3(b) and 3(d), and the optimal orthogonal and non-orthogonal steering vectors are selected according to (10).

Fig. 4 illustrates the data rates by perfect and non-orthogonal steering vectors, where the perfect steering vector is assumed to exactly compensate the AoA, i.e., $\phi_p = \phi_k$. Thus we have the maximal data rate shown as

$$R_{\max} = \log_2\left(1 + \frac{\alpha_0^2}{\sigma_z^2}\right). \tag{16}$$

In Fig. 4, the data rates vary a lot with different range of AoAs because in Fig. 3(b) the 16 beam patterns are not equally distributed in spatial frequency domain. The case of $\phi_p \sim \mathcal{U}(0^o, 15^o)$ $(0 \le \nu_p \le 2.07)$, is even 1 bit/s/Hz worse than the case of $\phi_p \sim \mathcal{U}(75^o, 90^o)$ $(7.73 \le \nu_p \le 8)$. Consider the channel bandwidth of 2.16 GHz at mmW systems [13], the data rates would dramatically decrease if the AoA changes from 80^o to 10^o when considering moving user terminal. Owing to the beam patterns are symmetric at 0^o, only the cases with $\phi_p \ge 0$ are simulated.

Then comparing Fig. 3(d) with Fig. 5, it can be seen that the data rates with different range of AoAs keep constant as we conclude in the previous section. The results in Fig. 5 are very close to the data rate by orthogonal steering vectors with $\phi_p \sim \mathcal{U}(-\frac{\pi}{2}, \frac{\pi}{2})$ in Fig. 6 because the deviation of the beamforming gain is almost up to 3 dB. In contrast, the averaged data rate by the non-orthogonal steering vectors with $\phi_p \sim \mathcal{U}(-\frac{\pi}{2}, \frac{\pi}{2})$ in Fig. 6 shows worse result since the data rates within $-15^0 < \phi_p < 15^o$ $(-2.07 \le \nu_p \le 2.07)$ are quite low.

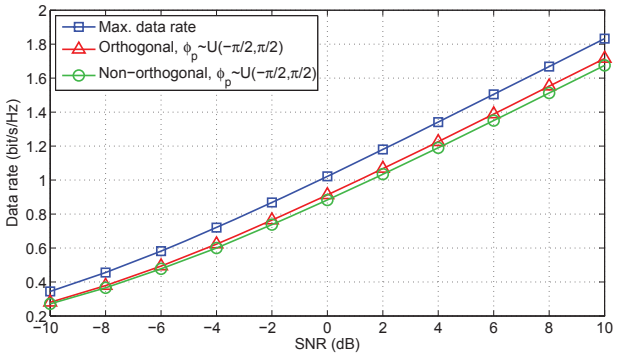

Figure 6: Comparison of achievable data rates by the perfect, the orthogonal, and the non-orthogonal steering vectors with uniformly distributed AoA over $(-\frac{\pi}{2}, \frac{\pi}{2})$.

The strategy of the design of the steering vectors can be extended to other practical applications, such as $N_K < N_R$. For example, $N_R = 16$ and $N_K = 4$, we can design the spatial frequency indices as $\nu_p = -6, -2, 2, 6$ (the corresponding steering angles are $\phi_p = -48.6, -14.5, 14.5, 48.6$). Designing the steering vectors in this way ensures the smallest deviation of the beamforming gain.

V. Conclusions

This paper elaborates why orthogonal steering vectors show better data rates than non-orthogonal ones by analyzing the steering angles, the steering spatial frequency indices, and beam patterns in spatial frequency domain. Due to the fact that the constant beamwidth values in spatial frequency domain, if the beam patterns are designed with uniformly distributed spatial frequency indices, which can ensure the smallest deviation of the beamforming gain. Orthogonal steering vectors satisfy this condition so that they can achieve higher data rates than non-orthogonal ones.

VI. Appendix

Given $\phi_p \sim \mathcal{U}(-\frac{\pi}{2}, \frac{\pi}{2})$, the cumulative distribution function (CDF) of ν_p ($\nu_p = \frac{N_R \cdot \sin\phi_p}{2}$) can be written as

$$\begin{aligned}
F_{\nu_p}(\nu_p) &= P\left(\nu_p \leq \nu_p\right) \\
&= P\left(\tfrac{N_R \cdot \sin\phi_p}{2} \leq \nu_p\right) \\
&= P\left(\phi_p \leq \sin^{-1}\left(\frac{2\nu_p}{N_R}\right)\right) \\
&= F_{\phi_p}\left(\sin^{-1}\left(\frac{2\nu_p}{N_R}\right)\right) \\
&= \int_{-\infty}^{\sin^{-1}(2\nu_p/N_R)} \frac{1}{\pi}\, d\phi_p \\
&= \int_{-\pi/2}^{\sin^{-1}(2\nu_p/N_R)} \frac{1}{\pi}\, d\phi_p \\
&= \begin{cases} 0, & \nu_p < -\frac{N_R}{2} \\ \frac{1}{\pi}\left(\sin^{-1}\left(\frac{2\nu_p}{N_R}\right) + \frac{\pi}{2}\right), & -\frac{N_R}{2} \leq \nu_p < \frac{N_R}{2} \\ 0, & \nu_p \geq \frac{N_R}{2} \end{cases}
\end{aligned}$$

By the rule for derivative of $\sin^{-1}(x) = 1/\sqrt{1-x^2}$, one has the pdf of ν_p,

$$f_{\nu_p}(\nu_p) = \begin{cases} 0, & \nu_p < -\frac{N_R}{2} \\ \frac{2}{\pi N_R \sqrt{1-(\frac{2\nu_p}{N_R})^2}}, & -\frac{N_R}{2} \leq \nu_p < \frac{N_R}{2} \\ 0, & \nu_p \geq \frac{N_R}{2} \end{cases}.$$

Acknowledgment

The research leading to these results has received funding from the European Union Seventh Framework Programme (FP7/2007-2013) under grant agreement n°619563 (MiWaveS).

References

[1] T. S. Rappaport, et al., Wireless Communications: Principles and Practice, 2nd Edition, Pearson Education, Upper Saddle River, NJ, 2002.

[2] T. A. Thomas, et al., "3D mmWave Channel Model Proposal," IEEE VTC Fall, 2014, pp. 1–6.

[3] T. S. Rappaport, et al., "Millimeter Wave Mobile Communications for 5G Cellular: It Will Work!," IEEE Access, Vol. 1, May 2013, pp. 335–349.

[4] A. Hajimiri, et al., "Integrated Phased Array Systems in Silicon," IEEE Proceedings, Vol. 93, Sep. 2005, pp. 1637–1655.

[5] J. C. Liberti, et al, "Smart Antennas for Wireless Communications: IS-95 and Third Generation CDMA Applications," Prentice Hall, NJ, 1999.

[6] L. Zhou and Y. Ohashi, "Efficient codebook-based MIMO beamforming for millimeter-wave WLANs," IEEE PIMRC 2012, pp. 9–12.

[7] D. Yang, et al., "DFT-Based Beamforming Weight-Vector Codebook Design for Spatially Correlated Channels in the Unitary Precoding Aided Multiuser Downlink," IEEE ICC, 2010, pp. 1–5.

[8] D. H. Johnson, et al, "Array Signal Processing: Concepts and Techniques," Prentice Hall, 1993.

[9] IEEE Std 802.11ad-2012. Part 11: Wireless LAN Medium Access Control (MAC) and Physical Layer (PHY) Specifications — Amendment 3: Enhancements for Very High Throughput in the 60 GHz Band, Dec. 2012.

[10] R, Kohno, et al., "Array Antenna Beamforming Based on Estimation of Arrival Angles Using DFT on Spatial Domain," IEEE PIMRC, 1991, pp. 38–43.

[11] J. L. Butler, et al., "Beam forming matrix simplifies design of electronically scanned antennas," Electronic Design, Vol. 9, Apr. 1961, pp. 170–173.

[12] D. Ramasamy, et al., "Compressive Adaptation of Large Steerable Arrays," IEEE Information Theory and Applications Workshop, 2012, pp. 234–239.

[13] IEEE Std 802.15.3cTM-2009, Part 15.3: Wireless Medium Access Control (MAC) and Physical Layer (PHY) Specifications for High Rate Wireless Personal Area Networks (WPANs) Amendment 2: Millimeterwave- based Alternative Physical Layer Extension, IEEE Computer Society, Oct. 2009.